Experimental verification of resonance instability bands in quadrupole doublet focusing channels

K. Fukushima, K. Ito, H. Okamoto, S. Yamaguchi,
K. Moriya, H. Higaki, T. Okano

Graduate School of Advanced Sciences of Matter, Hiroshima University 1-3-1 Kagamiyama, Higashi-Hiroshima 739-8530, Japan

S. M. Lund

Lawrence Livermore National Laboratory, Livermore, California 94550, USA

Abstract

The tabletop plasma trap experiment named "S-POD" is employed to explore the stability of intense charged-particle beams focused by a series of quadrupole doublet cells. The core of S-POD is a compact linear Paul-trap, where we generate a non-neutral ion plasma that can approximately reproduce the collective motion of an intense beam focused by periodic linear forces. Unlike conventional beam-dynamics experiments relying on large-scale transport channels and accelerators, it is straightforward in S-POD to control the functional form of beam focusing over a wide range of variation. We systematically measure the loss rate of trapped particles as a function of bare betatron tune and locate resonance bands in which the plasma becomes unstable. It is confirmed that a few bands of coherent resonances appear depending on the beam intensity. When there is an imbalance between the horizontal and vertical focusing, those instability bands split. Experimental results indicate that the instability band is insensitive to the phase of quadrupole focusing element placement within the doublet configuration. Experimental observations are compared with transverse slice particle-in-cell simulations carried out using the Warp code.

PACS numbers: 29.20.-c, 41.75.-i

1. Introduction

Almost all modern particle accelerator systems exploit the principle of strong focusing [1]. In strong focusing, both focusing and defocusing forces are employed in a manner where one can spatially confine a large number of charged particles more effectively than the case where only focusing forces are used [2, 3, 4]. The most standard strong focusing channel is the so-called "doublet lattice" in which the beam receives one linear focusing and one defocusing

quadrupole kick alternately within the lattice period [5]. A special case of the doublet with equal length focusing and defocusing quadrupoles axially spaced equidistantly within the lattice period is called a "FODO" lattice. FODO lattices make most efficient use of the quadrupole focusing strength, but have less free axial drift length within the period for other uses (pumping, diagnostics, etc). Quadrupole doublets are often adopted for beam transport channels and linear accelerators including a possible heavy ion fusion driver [6] and drift tube linacs [7]. A non-scaling fixed field alternating gradient ring also consists of many doublet cells [8]. This widespread use makes it important to understand the collective instabilities of high-quality hadron beams traveling in long doublet channels. While there are a number of numerical and analytic works on this subject in past literature [1, 9], little work has been carried out experimentally because of the practical reason of it being difficult to modify the focusing lattice in usual accelerator transport channels. In S-POD, this practical difficulty for accelerator systems in modifying the lattice is inconsequential since different lattice focusing elements can be synthesized electronically, thereby allowing us to systematically explore a wide variety of changes in lattice focusing functions.

In this paper, we investigate the space-charge effects in doublet focusing by employing a compact linear Paul trap system developed at Hiroshima University. Because the transverse collective motion of a non-neutral plasma in the trap is physically almost equivalent (beam-frame correspondence) to that of a charged-particle beam in strong focusing channels, we can use the trap to study transverse effects in beam transport [10]. The dedicated plasma trap system for beam physics applications is called "S-POD (Simulator for Particle Orbit Dynamics)" [11, 12]. After outlining S-POD experiments in Sec. 2, we show in Sec. 3 numerical simulation data in which the actual Paul trap configuration has been assumed. Experimental results from S-POD are then described in Sec. 4 and compared with the numerical simulations. To systematically explore the stability of ion beams focused by a series of doublets, we change the waveform of the plasma confinement field over a wide range. Concluding remarks are made in Sec. 5.

2. S-POD simulations of doublet focusing

Consider charged particles of mass m and charge state q confined in a linear Paul trap. The transverse collective motion of these particles is governed by the Hamiltonian

$$H = \frac{p_x^2 + p_y^2}{2} + \frac{1}{2}K(\tau)(x^2 - y^2) + \frac{q}{mc^2}\phi(x, y, \tau) \tag{1}$$

where ϕ is the scalar potential of Coulomb interactions among the particles, the independent variable is $\tau = ct$ with c being the speed of light, and $K(\tau)$ is the periodic focusing potential proportional to the radio-frequency (rf) voltages applied to the quadrupole electrodes. Equation (1) is identical in form to the Hamiltonian for the transverse betatron motion of an intense beam in a beam

transport channel, which means that we can make use of a non-neutral plasma in the trap for the study of beam dynamics in alternating-gradient (AG) transport channels. Detailed design considerations of a compact Paul trap for S-POD can be found in previous publications [13, 14]. A similar trap system for beam physics applications is also operating at Princeton Plasma Physics Laboratory where Gilson and co-workers have produced many interesting results [15, 16, 17].

Ideally, a step-function rf waveform as in Fig. 1(a) is desired to emulate piecewise-constant quadrupole doublet focusing in a Paul trap. Such piecewise constant models for $K(\tau)$ rather than a specific axial fringe function for a magnet focusing technology are often employed in an "equivalent" sense to represent an idealization in analysis of beam transport [18]. As displayed in Fig. 1(b), it is possible for the rf system of S-POD to approximately generate such rf power consistent with piecewise constant $K(\tau)$. We, however, experimentally observe that the maximum number of trappable ions tends to be lower with the step-function voltage, compared to confinement with a sinusoidally varying $K(\tau)$. The reason is presently unknown, but we suspect that low-frequency noise included in the applied periodic voltage may be responsible for the observed reduction in plasma density. In addition, the rise (and fall) time of a pulse voltage is limited to $10 \sim 20$ nsec in our power supply system while the ideal pulse width for 50% filling is only 250 nsec at the operating frequency of 1 MHz. The ratio of the rise (fall) time to the pulse width becomes worse as we reduce the filling factor. Considering these technical issues, we here take a sinusoidal model; namely, we extract up to four fundamental Fourier harmonics from the ideal doublet waveform and apply them to the quadrupole electrodes. This model simplification is expected to have no essential effect on the basic mechanism of coherent resonances because the instability occurs when the frequency of a certain collective mode equals one of the driving harmonic frequencies. It should not matter whether the driving force includes many other harmonics. The use of simple sinusoidal rf waves makes it much easier for us to design the necessary power-supply and control systems for systematic experiments.

For later convenience, we introduce several geometric parameters as illustrated in Fig. 1. We denote $\ell_{\rm F}$ and $\ell_{\rm D}$ as the widths of focusing and defocusing pulses in the horizontal x-direction. The heights of the two square pulses are set equal. The distance between the focusing to the defocusing pulses, i.e., the gap width, is denoted as g, and the length of single focusing period as L. The so-called *filling factor* (or *quadrupole occupancy factor*) is given by $\xi = (\ell_{\rm F}+\ell_{\rm D})/L$. Another parameter of interest to us is defined by $\zeta = g/(L-g-\ell_{\rm F}-\ell_{\rm D})$ that we refer to as the *drift ratio*. ζ measures asymmetry of the gaps in the quadrupole doublet ($\zeta = 1$ corresponds to a symmetric FODO). Expanding the doublet waveform as in Fig. 1 into Fourier series, we obtain

$$K(\tau) = \sum_{n=1}^{\infty} A_n \sin(2\pi n\tau/L + \alpha_n) \tag{2}$$

where A_n and α_n are the amplitude and phase of nth Fourier harmonic. In the present experiments, we pick a few of low harmonic Fourier components

and apply them simultaneously to the quadrupole electrodes to see if any new stop bands appear depending on which harmonics are chosen. We have so far considered the case where the plasma is focused primarily by the first ($n = 1$) harmonic that has the frequency of 1 MHz. The rf amplitude required for the full survey of the tune space is then less than about 93 volts for Ar^+ ions. Other harmonics of higher frequencies are treated as perturbation due to a technical reason that limits the maximum amplitudes of these additional harmonic components [19]. The amplitude of each perturbation harmonic is typically set at a few percent of the primary focusing-wave amplitude.

3. Numerical predictions from Warp simulations

Before proceeding to experimental simulations with S-POD, it is informative to examine numerically whether we find any essential difference between the ideal doublet focusing with a piecewise constant focusing function and the present simplifying model with only a few harmonics. As mentioned above, the amplitudes of higher-frequency harmonics are limited in the actual experiment and thus lower than the ideal values necessary to accurately represent the desired piecewise constant focusing force. This fact makes it more important to carry out systematic numerical simulations for comparison. The particle-in-cell (PIC) code "Warp" has been employed for this purpose [20, 21]. Since we are particularly interested in transverse betatron resonances, an axially uniform plasma is effectively assumed in transverse slice Warp simulations to ignore the longitudinal dynamics.

The Warp simulations were carried out in a transverse xy-slice mode where effective longitudinal energy spread is neglected. An initial "pseudo-equilibrium" distribution matched to the periodic focusing channel was formed by canonically transforming a root-mean-squared (rms) equivalent thermal equilibrium distribution constructed under the smooth approximation [22]. This initial distribution reflects self-consistent Debye screening due to space charge in the beam core and avoids potentially spurious instabilities associated with initial Kapchinsky-Vladimirsky (KV) distributions in periodic focusing channels when space charge is strong [23]. 400 advance steps per doublet period were employed to resolve higher harmonic variations of the applied focusing force with the quadrupole bias potential applied consistently with the relevant harmonics in eq. (2) to the actual electrode arrangement used in the experiment as described in ref. [24]. Approximately 700 grid cells are employed across the rms equivalent beam to resolve space-charge variations and applied field nonlinearities. Simulations use 10^5 particles for good statistics with $\sim$150 particles per grid cell and $\sim 2 \times 10^4$ particles in a circle formed from the thermal Debye length (rms equivalent beam measures). In the Warp simulations we employ rms emittance growth (x- and y-plane averaged measure) relative to the initial value over an evolution of 100 periods to identify bands of instability. Over this simulation length there are generally no particle losses. For the case of strong instability, longer evolutions may result in significant particle losses. For weaker instability, losses may be

modest or negligible before the instability nonlinearly saturates. In the experiment we expect losses to be enhanced in the case of instability due to a cascade of processes involving effects such as misalignments, noise, and scattering.

Let us start from the symmetric FODO case where $\zeta = 1$. Figure 2 shows the resonance instability bands identified by Warp simulations. Three different linear focusing functions illustrated in the upper panel have been taken for example. The tune depression is defined by $\eta = 1-\Delta\nu/\nu_0$ where ν_0 is the bare tune per single focusing period and $\Delta\nu$ is the rms tune shift caused by the Coulomb repulsion. For an equilibrium plasma with the rms emittance $\varepsilon_{\rm rms}$, the space-charge-depressed tune can be evaluated from $\nu \equiv \nu_0 - \Delta\nu = \oint(\varepsilon_{\rm rms}/2\pi r_\perp^2)d\tau$ where $r_\perp$ denotes the transverse rms extent of the plasma. The ordinate of Fig. 2 is the plane-averaged emittance growth after the plasma is stored in the Paul trap for 100 focusing periods at a fixed tune. Obviously, emittance growth obtained which corresponds to the location of instability is very insensitive to the form of the focusing insofar as equivalent values of focusing strength measured by ν_0 are employed. We recognize three clear peaks of emittance growth near $\nu_0 \approx 1/6, 1/4$, and $1/3$ which is consistent to previous numerical and experimental results [12, 25]. According to the Vlasov theory in ref. [26], the major peak of emittance growth near $\nu_0 \approx 1/4$ is generated mainly by the instability of the linear collective mode, while the other two near $\nu_0 \approx 1/6$ and $1/3$ are due to third-order nonlinear resonances. These stop bands are significantly enhanced when the external driving field contains nonlinear force terms [25].

We now change both the filling factor and drift ratio to $\xi = 0.25$ and $\zeta = 0.1$, keeping the other numerical conditions identical. The upper panel in Fig. 3 shows the focusing waveforms corresponding to these parameters. The blue curve consists of the Fourier components with the harmonic number $n = 1, 2, 3$, and 4; unlike the previous example in Fig. 2, the even harmonics are allowed. Corresponding Warp simulation results are given in the lower panel. Although the three curves do not perfectly overlap, we still observe the three significant instability bands rising near $\nu_0 \approx 1/6, 1/4$, and $1/3$ in all cases. For more information, the stop band distribution under the single sinusoidal focusing is compared with those under the ideal doublet waveforms that have different filling factors and drift ratios. Figure 4 suggest that the emittance growth is not substantially affected by the changes in ξ and ζ. According to a number of systematic Warp simulations executed under various conditions, the simple sinusoidal-focusing model can well reflects the resonance nature of an arbitrary doublet focusing.

4. Results from S-POD experiments

Non-neutral plasmas can readily be produced by ionizing neutral gas atoms with a low-energy electron beam from an electron gun. We have often chosen Ar for S-POD experiments. It is possible to change the initial plasma density to some degree by controlling the gas pressure and electron beam current. An rms tune depression of $\eta \approx 0.8$ can be reached with the present S-POD apparatus. In the following experimental data, Ar^+ ions are confined in the Paul trap typically

for 10 msec which corresponds to a beam propagation length of 10,000 doublet cells. Ions surviving after the 10-msec storage are then dumped from the trap and measured in a Faraday cup. More details of the plasma formation process and plasma measurement can be found in refs [11] and [24]. The computer control system for S-POD automatically repeats this measurement cycle, slightly shifting the operating tune (in other words, the amplitudes of the sinusoidal focusing fields) every machine cycle. A single cycle (including data transfer to a PC) is completed within 10 seconds. Since the fundamental harmonic oscillates at 1 MHz, the frequency of the nth harmonic superimposed on it is n MHz.

4.1. Symmetric focusing

In the usual operating mode of a linear Paul trap, the time variations of the horizontal (x) and vertical (y) plasma confinement potentials are completely symmetric. The two transverse tunes (ν_{0x}, ν_{0y}) are then equal, i.e., $\nu_{0x} = \nu_{0y} (= \nu_0)$, as assumed in the last section. Figure 5 shows the stop-band distribution measured with S-POD under the symmetric focusing condition. In order to experimentally verify the Warp prediction in Fig. 2, we have taken the first four odd harmonics into consideration. The amplitudes of these higher-frequency harmonics are, however, fixed at 5 % of the amplitude of the primary focusing harmonic ($n = 1$) because of a technical limitation [19]. The black line corresponds to the case where the three perturbation harmonics with $n = 3, 5,$ and 7 are simultaneously applied to the quadrupole rods in addition to the fundamental $n = 1$ harmonic. These perturbation waves oscillate at 3, 5, and 7 MHz. The ordinate indicates the number of Ar^+ ions detected by the Faraday cup after a storage period of 10 msec. The initial ion number $N_{\rm in}$ is set at either 10^6 or 10^7 to check density-dependent effects. We confirm the existence of three bands of particle loss near $\nu_0 \approx 1/6, 1/4,$ and $1/3$, which agrees with the Warp results in Fig. 2 [27]. When $N_{\rm in}$ is increased, all these stop bands shift toward the higher tune side due to the stronger Coulomb repulsion that depresses the effective tune. The estimated tune depression at $N_{\rm in} \approx 10^7$ is about 0.8 [11]. For comparison, the stop-band distribution when all three higher harmonics are switched off is plotted in red, but no significant change in particles stored is observed. Results of another experiment are given in Fig. 6. The plasma is now focused by the first four Fourier harmonics with $n = 1, 2, 3,$ and 4 (instead of $n = 1, 3, 5,$ and 7 in Fig. 5). We again observe no substantial difference from the stop-band distribution in the single harmonic focusing (red curve), as anticipated from extrapolations of emittance growth bands in the Warp simulations. We also tried other simpler cases in which only a single high-frequency harmonic is superimposed with the fundamental focusing wave of $n = 1$, but the results remained unchanged.

4.2. Asymmetric focusing

It is technically easy to obtain different horizontal and vertical bare tunes in the S-POD apparatus by applying static bias voltages of quadrupole symmetry to the four electrodes. For instance, if the two horizontal electrodes are biased

with a certain positive DC voltage $V_{\rm DC}$, then the horizontal tune ν_{0x} for positively charged ions becomes larger than the vertical tune ν_{0y}. The difference $\delta\nu(\equiv \nu_{0x} - \nu_{0y})$ between the two tunes depends on $V_{\rm DC}$ and the amplitudes of the focusing harmonics. Particle-loss distributions near the quarter integer, obtained under the asymmetric focusing conditions, are shown in Fig. 7. We here activate no higher-frequency harmonics, recalling that the single sinusoidal focusing can well approximate general doublet focusing. It is evident that the asymmetric focusing gives rise to instability band splitting. This observation is quite reasonable because ν_{0x} and ν_{0y} now approach a certain rational number at different rf amplitudes. In Fig. 7, $\delta\nu$ is adjusted to various different values by choosing proper $V_{\rm DC}$ and rf amplitude. The stop band staying at $\nu_{0x} \approx 0.265$ in all cases is attributed to the horizontal resonance. The vertical stop band of the corresponding order moves as the abscissa is ν_{0x} (not ν_{0y}) in this plot. We recognize that the size of the stop-band shift agrees with $\delta\nu$. When $\delta\nu = 0$, the two stop bands merge together leading to enhanced ion losses. It has been confirmed through Warp simulations that simulated emittance growth near $\nu_0 \approx 1/6$ and $1/3$ also shows corresponding behavior to the experimental loss curves when $\delta\nu$ is finite.

Varying the bias $V_{\rm DC}$ and the amplitude of the sinusoidal focusing wave over a wide range, we can clarify possible beam instability regions in the tune space. Such a tune diagram is constructed in Fig. 8 at $N_{\rm in} \approx 10^6$ (black) and $N_{\rm in} \approx 10^7$ (red). We again pay attention to the tune domain where the strong linear collective resonance should take place. The full width at half maximum (FWHM) of the band of particle loss is roughly evaluated from the S-POD data at each operating point and expressed with a bar in the picture. A dot in the bar indicates the location at which ion losses are maximum. We clearly see two instability bands crossing near the point where $\nu_{0x} = \nu_{0y} = 1/4$. These stop bands are always located slightly above the quarter integer, i.e., in the region $\nu_{0x(0y)} \geq 1/4$ because of the space-charge-induced tune shift. Since the tune of the linear collective mode is more depressed at higher ion density, the shift becomes larger as we increase $N_{\rm in}$. The stop bands are considerably widened for $N_{\rm in} \approx 10^7$ analogously to the case demonstrated in Figs. 5 and 6. We also notice that at high density, the point of maximum ion losses always deviates from the stop-band center to the low tune side. This is because the operating point stays longer within the stop band when it is near the low-tune edge at the beginning. Once the resonant instability is activated, the plasma emittance grows resulting in a density reduction or even ion losses. The whole stop band then moves toward the lower tune side. Therefore, the ion-loss rate within a particular stop band is more enhanced for the operating point that has a smaller bare tune.

5. Summary

We have studied the resonance nature of an intense charged-particle beam propagating through periodic quadrupole doublet focusing channels. Unlike conventional approaches where it is generally difficult to reconfigure beam transport

lattices of limited length, we here made use of the novel tabletop tool "S-POD" that enables systematic *experimental* simulations of beam propagation under a diverse range of external periodic focusing potentials. A large number of heavy ions were stored in a compact linear Paul trap for a certain period to reproduce the collective beam behavior over thousands of doublet focusing periods. When the horizontal and vertical net focusing effects were equal ($\nu_{0x} = \nu_{0y}$), three noticeable stop bands appeared near the bare tunes $\nu_0 \approx 1/6, 1/4$, and $1/3$ [25]. According to the coherent resonance theory in ref. [26], the relatively large stop band slightly above $\nu_0 \approx 1/4$ is due mainly to the instability of the quadrupole mode while the sextupole resonance should be responsible for the other two. Despite the fact that nonlinear driving forces are probably enhanced by finite electrode misalignments, we found no other sharp instability bands originating from higher-order resonances in either the simulations (via location of emittance growth) or in the laboratory experiment (via measured particle losses). The observed instability distribution was not essentially influenced by the choice of higher-frequency Fourier harmonics in the plasma confinement field but slightly shifted depending on the plasma intensity. These experimental observations agree fairly well with two-dimensional Warp simulations. We can conclude that the ideal doublet focusing is dynamically similar to the simple sinusoidal focusing, regardless of the filling factor ξ and drift ratio ζ. At least, the locations of major stop bands are quite insensitive to the details of the doublet structure. We also confirmed that each of the three stop bands splits into two parts when the transverse tunes are different ($\nu_{0x} \neq \nu_{0y}$). This is not surprising because a resonance occurs under the condition that either ν_{0x} or ν_{0y} is close to a certain rational number. One of the two parts should thus be caused by a horizontal resonance and the other by a vertical resonance of the same order.

Acknowledgments

The present work was supported in part by a Grant-in-Aid for Scientific Research, Japan Society of the Promotion of Science. The authors wish to thank D. P. Grote for support with the Warp simulations and H. Sugimoto for assistance starting early phases of the simulations.

References

[1] See, e.g., A. W. Chao and M. Tigner (Ed.), *Handbook of Accelerator Physics and Engineering* (World Scientific, Singapore, 1999) and references therein. ISBN 981-02-3500-.

[2] E. D. Courant, H. S. Snyder, Theory of the Alternating-Gradient Synchrotron, Annals of Physics 3 (1958) 1.

[3] N. C. Christofilos, unpublished manuscript (1950); U.S. Patent No. 2.736,799 (1956).

[4] E. D. Courant, M. S. Livingston, H. Snyder, The Strong-Focusing Synchroton-A New High Energy Accelerator, Phys. Rev. 88 (1952) 1190.

[5] H. Wiedemann, Particle Accelerator Physics: Basic Principles and Linear Beam Dynamics, Springer-Verlag, New York, 1993.

[6] See, e.g., the Proceedings of the 17th International Symposium on *Heavy Ion Inertial Fusion*, Nucl. Instr. Meth. A 606, Issues 1 - 2. pp. 1 - 232 (2009).

[7] T. Wangler, Principles of RF Linear Accelerators, John Wiley & Sons, New York, 1998.

[8] S. Machida *et al.*, Acceleration in the Linear Non-Scaling Fixed-Field Alternating-Gradient Accelerator EMMA, Nature Physics 8 (2012) 243.

[9] M. Reiser, Theory and Design of Charged Particle Beams, John Wiley & Sons, New York, 1994.

[10] H. Okamoto, H. Tanaka, Proposed Experiments for the Study of Beam Halo Formation, Nucl. Instr. Meth. A 437 (1999) 178.

[11] S. Ohtsubo, M. Fujioka, H. Higaki, K. Ito, H. Okamoto, H. Sugimoto, S. M. Lund, Experimental Study of Coherent Betatron Resonances with a Paul Trap, Phys. Rev. ST Accel. Beams 13 (2010) 044201.

[12] H. Okamoto, M. Endo, K. Fukushima, H. Higaki, K. Ito, K. Moriya, S. Yamaguchi, S. M. Lund, Radio-Frequency and Magnetic Trap Simulations of Beam Propagation Over Long Paths, in this proceedings.

[13] H. Okamoto, Y. Wada, R. Takai, Radio-Frequency Quadrupole Trap as a Tool For Experimental Beam physics, Nucl. Instr. Meth. A 485 (2002) 244.

[14] R. Takai, H. Enokizono, K. Ito, Y. Mizuno, K. Okabe, H. Okamoto, Development of a Compact Plasma Trap for Experimental Beam Physics, Jpn. J. Appl. Phys. 45 (2006) 5332.

[15] R. C. Davidson, Q. Qian, G. Shvets, A Paul Trap Configuration to Simulate Intense Non-Neutral Beam Propagation Over Large Distances Through a Periodic Focusing Quadrupole Magnetic Field, Phys. Plasmas 7 (2000) 1020.

[16] E. P. Gilson, M. Chung, R. C. Davidson, P. C. Efthimion, R. Majeski, Paul Trap Simulator Experiment to Model Intense-Beam Propagation in Alternating-Gradient Transport Systems, Phys. Rev. Lett. 92 (2004) 155002.

[17] E. P. Gilson, M. Chung, R. C. Davidson, P. C. Efthimion, R. Majeski, Transverse Beam Compression on the Paul Trap Simulator Experiment, Phys. Rev. ST Accel. Beams 10 (2007) 124201.

[18] S. M. Lund, B. Bukh, Stability Properties of the Transverse Envelope Equations Describing Intense Ion Beam Transport, Phys. Rev. ST Accel. Beams 7 (2004) 024801.

[19] The sum of the additional rf voltages must have an amplitude below about 15 V that is determined by the ability of the currently-used OP amp.

[20] D. P. Grote, Three Dimensional Simulations of Space Charge Dominated Heavy Ion Beams with Applications to Inertial Fusion Energy, Ph.D. thesis, University of California at Davis (1994).

[21] D. P. Grote, A. Friedman, G. D. Craig, I. Haber, W. M. Sharp, Progress Toward Source-to-Target Simulations, Nucl. Instr. Meth. A 464 (2001) 563.

[22] S. M. Lund, T. Kikuchi, R. C. Davidson, Generation of Initial Kinetic Distributions for Simulation of Long-Pulse Charged Particle Beams with High Space-Charge Intensity, Phys. Rev. ST Accel. Beams 12 (2009) 114801.

[23] I. Hofmann, L. J. Laslett, L. Smith, I. Haber, Stability of the Kapchinskij-Vladimirskij (K-V) Distribution in Long Periodic Transport Systems, Particle Accelerators 13 (1983) 145.

[24] H. Sugimoto, Multi-Particle Simulation Studies on the Generation and Stability of High-Density Coulomb Systems, Ph.D. thesis, Hiroshima University (2011).

[25] H. Takeuchi, K. Fukushima, K. Ito, K. Moriya, H. Okamoto, H. Sugimoto, Experimental Study of Resonance Crossing with a Paul Trap, Phys. Rev. ST Accel. Beams 15 (2012) 074201.

[26] H. Okamoto, K. Yokoya, Parametric Resonances in Intense One-Dimensional Beams Propagating Through a Periodic Focusing Channel, Nucl. Instr. Meth. A 482 (2002) 51–64.

[27] Any Paul traps have finite electrode misalignments that can enhance nonlinearities in the plasma confinement field. The third-order stop band near $\nu_0 \approx 1/3$ should thus be somewhat enlarged compared to the ideal linear focusing situation.

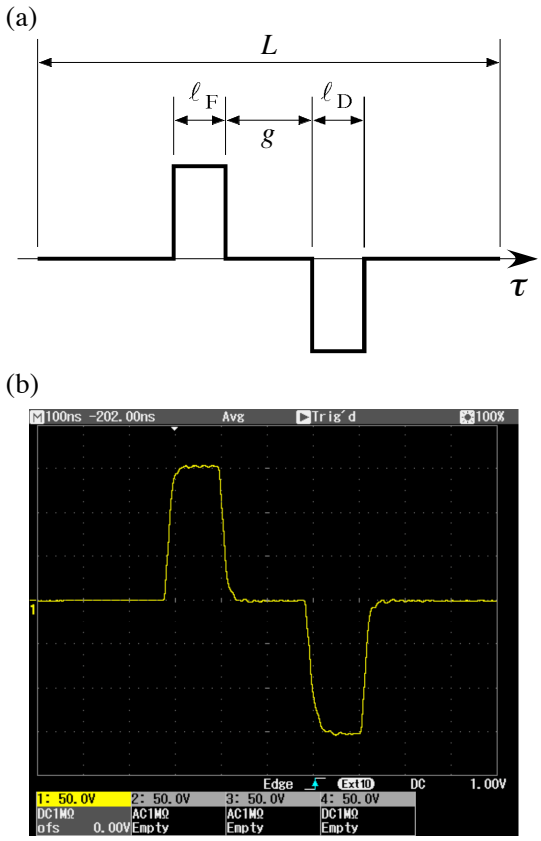

Figure 1: Doublet waveform for transverse beam focusing. (a) Ideal focusing function $K(\tau)$ for a period L. The amplitudes of the two (focusing and defocusing) pulses are equal. (b) The corresponding measured rf voltage generated by the S-POD rf power supply system. The frequency is set at 1 MHz and the full width of the picture is 1 μs.

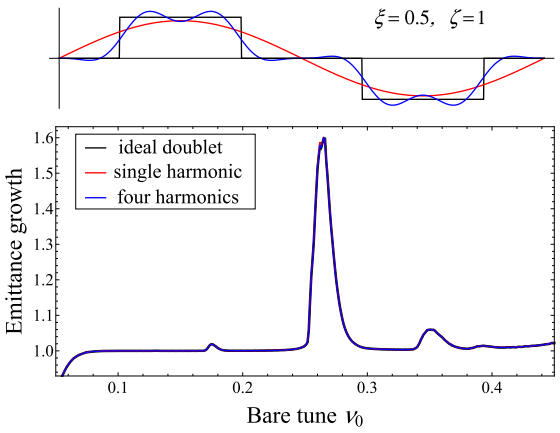

Figure 2: Warp simulation results corresponding to three different waveforms for $K(\tau)$. The three curves in the upper picture illustrate the linear focusing function considered in this example: the ideal piecewise constant doublet with $\xi = 0.5$ and $\zeta = 1$ (black), a single sinusoidal harmonic (red), and an approximate doublet (blue) composed from the first four Fourier components ($n = 1, 3, 5, 7$). Note that only odd harmonics appear in the symmetric case with $\zeta = 1$. Root-mean-squared emittance growth obtained after 100 focusing periods with these focusing waveforms are plotted in the lower panel as a function of the bare tune ν_0. A thermal equilibrium distribution with the rms tune depression of 0.9 has been assumed initially. The three Warp results almost completely overlap with each other.

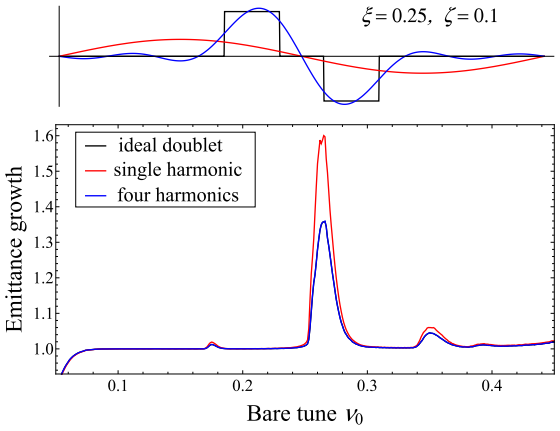

Figure 3: Warp simulation results corresponding to three different waveforms for $K(\tau)$. The simulation parameters here are the same as those in Fig. 2, except the filling factor and drift ratio are changed to $\xi = 0.25$ and $\zeta = 0.1$. The blue focusing curve is composed from the four harmonics with $n = 1, 2, 3$, and 4.

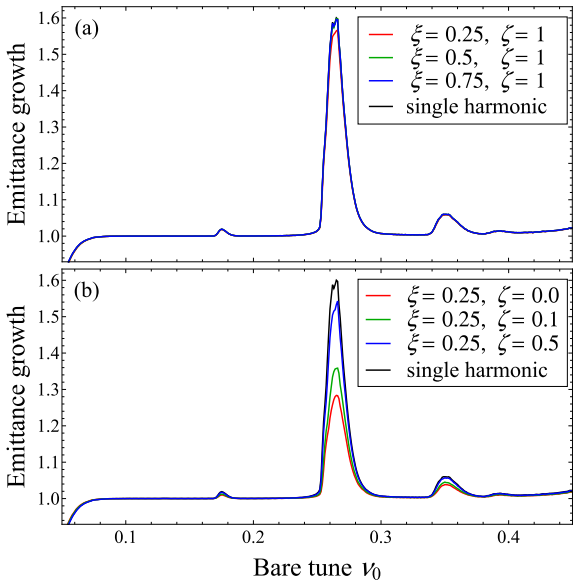

Figure 4: Warp simulation results obtained with the ideal doublet focusing with various values of ξ and ζ as indicated. (a) ξ-dependence of emittance growth bands when $\zeta = 1$. (b) ζ-dependence of emittance growth bands when $\xi = 0.25$. The band distribution for the single-harmonic sinusoidal focusing is plotted with a black solid curve for comparison in both panels.

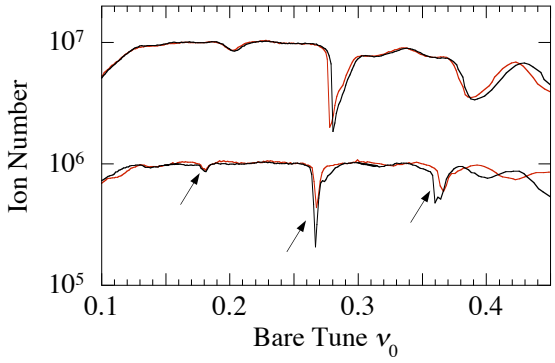

Figure 5: Particle-loss distribution measured in S-POD. Similarly to the numerical example in Fig. 2, three weak harmonics with $n = 3, 5$, and 7 are superimposed on the primary focusing harmonic ($n = 1$). The amplitudes of the perturbation harmonics are fixed at 5% of the first $n = 1$ harmonic amplitude. The ordinate of the picture represents the number of Ar^+ ions surviving after a 10-msec storage (10^4 periods) at a fixed tune in the Paul trap. The initial number of Ar^+ ions is set at $N_{in} \approx 10^6$ (lower curve) or 10^7 (upper curve). For reference, the particle-loss distributions obtained without the perturbation harmonics are plotted in red. The arrows indicate locations of the three loss bands induced mainly by the second and third-order resonances.

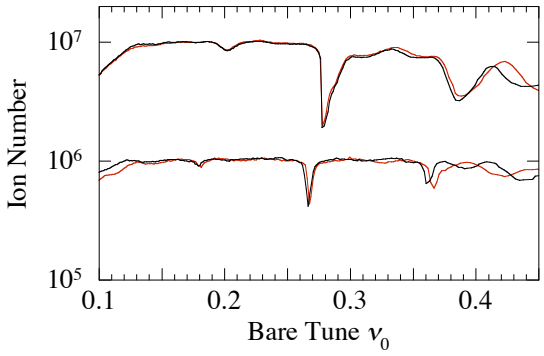

Figure 6: Particle-loss distribution measured in S-POD. Similarly to the numerical example in Fig. 3, three weak harmonics with $n = 2, 3$, and 4 are superimposed on the primary focusing harmonic ($n = 1$). Other conditions are identical to those in Fig. 5. Black and red curves show the particle-loss distributions with and without the perturbation harmonics.

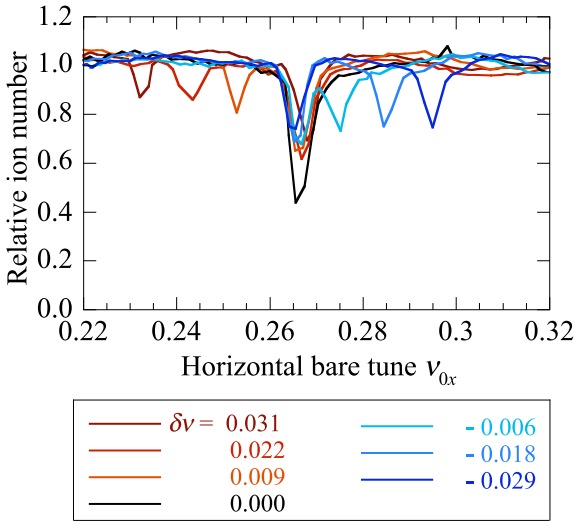

Figure 7: Linear-instability-induced particle loss bands measured under asymmetric focusing conditions. The number of Ar^+ ions surviving after a 10-msec storage in the Paul trap is plotted as a function of the horizontal bare tune ν_{0x}. The higher-frequency harmonics have been switched off in this experiment; the plasma is focused by the single sinusoidal field oscillating at 1 MHz. $N_{\rm in}$ is set at 10^6. The imbalance between the transverse bare tunes (ν_{0x}, ν_{0y}) is introduced by biasing the quadrupole rods with DC voltages. Seven different cases of tune separation are shown with values as indicated in the color coded key.

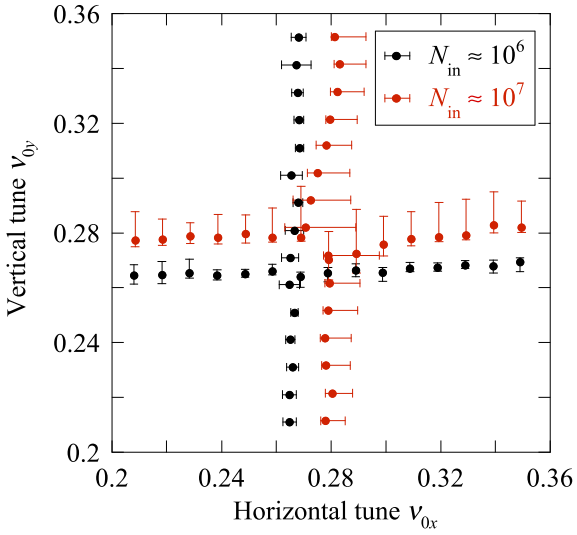

Figure 8: Tune diagram of particle loss bands in the vicinity of a quarter integer for two plasma intensities. The location of the linear resonance stop band obtained through ion-loss measurements in S-POD is plotted on the tune space. Horizontal or vertical bars represent the approximate FWHM of the loss band estimated from the measurement data. A dot on each bar shows where maximum ion losses occur within the band. Two different initial ion numbers are considered, $N_{\rm in} \approx 10^6$ (black) and 10^7 (red). The plasma confinement time is set at 10 msec in all measurements.